CHALMERS
UNIVERSITY OF TECHNOLOGY

Validation of high-fidelity simulation-based safe operating envelopes for articulated heavy vehicles using real test data

Vehicle System Dynamics
International Journal of Vehicle Mechanics and Mobility

ISSN: (Print) (Online) Journal homepage: https://www.tandfonline.com/loi/nvsd20

Validation of high-fidelity simulation-based safe operating envelopes for articulated heavy vehicles using real test data

Umur Erdinc, Mats Jonasson, Maliheh Sadeghi Kati, Bengt Jacobson, Jonas Fredriksson & Leo Laine

To cite this article: Umur Erdinc, Mats Jonasson, Maliheh Sadeghi Kati, Bengt Jacobson, Jonas Fredriksson & Leo Laine (07 Jan 2024): Validation of high-fidelity simulation-based safe operating envelopes for articulated heavy vehicles using real test data, Vehicle System Dynamics, DOI: 10.1080/00423114.2023.2296595

To link to this article: https://doi.org/10.1080/00423114.2023.2296595

VEHICLE SYSTEM DYNAMICS
https://doi.org/10.1080/00423114.2023.2296595

Validation of high-fidelity simulation-based safe operating envelopes for articulated heavy vehicles using real test data

Umur Erdinc [a,b], Mats Jonasson [a], Maliheh Sadeghi Kati [b], Bengt Jacobson [a], Jonas Fredriksson [c] and Leo Laine [a,d]

[a]Department of Mechanics and Maritime Sciences, Chalmers University of Technology, Gothenburg, Sweden; [b]Vehicle Motion and Thermal Management, Volvo Group Trucks Technology, Gothenburg, Sweden; [c]Department of Electrical Engineering, Chalmers University of Technology, Gothenburg, Sweden; [d]Safe and Efficient Driving, Volvo Group Trucks Technology, Gothenburg, Sweden

ABSTRACT

The electrification of towing and trailing units creates new torque allocation alternatives among different units of articulated heavy vehicles. To increase the power and energy efficiency, control algorithms can request propulsion or regenerative braking from a single unit while keeping the other units unbraked or unpropelled. However, this may lead to safety problems, such as jackknifing or trailer swing. This paper uses a high-fidelity simulation tool to formulate safe operating envelopes for a tractor and semitrailer combination for braking-in-turn cases. The effects of different vehicle and environment parameters on the safe operating envelope are studied. The safe operating envelope obtained is then validated using real vehicle tests and can be used with any control algorithm to avoid requesting unsafe unit force combinations.

ARTICLE HISTORY
Received 9 February 2023
Revised 16 October 2023
Accepted 5 December 2023

KEYWORDS
Yaw instability; jackknifing; trailer swing; combination spin-out; articulated heavy vehicle; electric vehicle; safe operating envelope

1. Introduction

In recent decades, there have been rapid developments in articulated heavy vehicles (AHVs). These vehicles are attractive alternatives to single-unit trucks due to their significant commercial and environmental benefits for transporting goods [1–3]. However, their poor lateral stability at high speeds and risk of unstable motion modes on low friction surfaces, including jackknifing, trailer swing and rollovers, have raised serious safety concerns regarding highway safety and fatal accidents [4–8]. For instance, according to the Federal Motor Carrier Safety Administration's (FMCSA) data, in 2020, 5.7% of all fatal AHV accidents in the US involved jackknifing [9].

With the electrification of tractors and trailing units, modern AHVs can use both towing units and trailing units for propulsion. Furthermore, due to power and energy efficiency concerns, modern AHVs can achieve propulsion and regenerative braking with a single unit. Applying propulsion or brakes to just one unit may result in a loss of traction and cause stability problems. Thus, focussing on the stability of the AHVs becomes even more important, given the recent trend towards electrification. Furthermore, to avoid

CONTACT Umur Erdinc umur.erdinc@volvo.com

This article has been corrected with minor changes. These changes do not impact the academic content of the article.

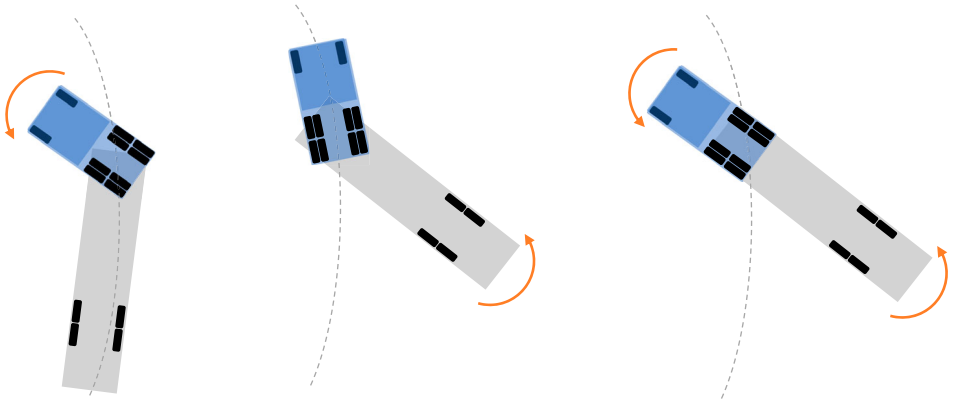

(a) Jackknifing (b) Trailer swing (c) Combination spin-out

Figure 1. Illustrations of different yaw instabilities for a tractor (blue) and semitrailer (grey) [11]. (a) Jackknifing, (b) Trailer swing and (c) Combination spin-out.

the controllers requesting unsafe propulsion and braking forces for different units, a 'safe operating envelope (SOE)' is needed for multi-unit vehicle control.

AHVs may experience two types of instability: static (divergent) instability or dynamic instability. Static instability occurs when the states (such as yaw rate) of the AHV grow exponentially with no oscillations. Dynamic instability, on the other hand, occurs if the states have oscillations with increasing magnitude (like in trailer sway) [10]. This paper focuses only on the static yaw instabilities of AHVs with a tractor and semitrailer: tractor jackknifing, trailer swing, and combination spin-out.

Tractor jackknifing occurs when the rear wheels of the tractor lose traction; trailer swing occurs when the trailer wheels lose traction. Loss of traction usually occurs due to poor slip control during hard braking with too deep slip. However, it can also occur during propulsion and is especially common on slippery roads. If both towing and trailing units lose traction and begin sliding, then combination spin-out occurs. These three unstable modes of AHVs are shown in Figure 1 [11].

G-g diagrams, also known as 'acceleration envelope', are well-established tools that are often used for illustrating the maximum achievable longitudinal and lateral accelerations of a vehicle [12–14]. It is also common to use the vehicle velocity to create 'g-g-v' diagrams due to the velocity-dependent nature of the accelerations. These diagrams are commonly used to assess vehicle performance and study lap times. However, their application in defining the safety limits of the AHVs has been relatively limited.

On the other hand, SOEs are widely used in various areas such as aircraft [15–18], submarines [19] and nuclear plants [20]. In the automotive field, SOEs are used to avoid yaw instabilities and usually limit the side-slip angles and yaw rates of single-unit vehicles [21–25]. For instance in [26], an SOE is defined for a tractor and semitrailer combination, primarily focussing on electric trailer propulsion.

In recent work [11], an SOE was defined for multi-unit vehicles, specifying upper and lower limits for the actuator requests, typically related to propulsion and braking forces. The SOE is determined as a function of vehicle states such as lateral acceleration or longitudinal speed, and as well as environmental parameters like road slope or road friction.

Control algorithms using SOE enable the vehicle to operate more safely, avoiding improper actuator requests that could lead to yaw instabilities. In this study, a nonlinear single-track model and a tyre model (linear within the friction circle) were employed to simulate various combinations of tractor and semitrailer braking and propulsion forces at different lateral accelerations [11]. Each manoeuvre was classified as safe or unsafe based on the side-slip angle deviations in each unit. Furthermore, the vehicle model was linearised and stability analyses were performed for different yaw instability modes, and the impact of different parameters on yaw stability was assessed. A single-track model is identified as a computationally efficient way to perform many simulations and obtain an SOE online on the vehicles' electronic control units.

High-fidelity models provide more precise representations of the AHVs but demand significantly more computational time than simpler models. An alternative involves offline simulations using high-fidelity vehicle models, exploring a wide range of scenarious involving various parameters. These precomputed SOEs are then stored in the AHV's memory and are integrated with the control algorithm of the vehicle. The selected control algorithm can be either a simple rule-based controller or a closed-loop controller [27]. In the latter case, the SOE acts as an initial safety layer, and if it cannot ensure safety, a closed-loop controller can take over.

In this paper, the SOE concept introduced in [11] will be studied in detail. Instead of using a simpler model like the one in [11], a high-fidelity model will be used to obtain the SOE. This newly obtained SOE then can be used to validate the SOEs obtained with simpler models. Furthermore, the effects of different parameters on the SOE will be studied and corresponding SOEs will be shown. Finally, validation of the SOE obtained by using a high-fidelity vehicle model will be presented, with real vehicle test results. Thus, it will be shown that an SOE obtained by simulations is accurate and safe to be used in real vehicles despite some significant modelling challenges and the stochastic real-world conditions.

2. Simulation-based derivation of SOE

In this section, the SOEs for braking-in-turn scenarios are obtained through numerical simulations performed on a high-fidelity vehicle model and the sensitivity of the SOE to various parameters is investigated.

2.1. Manoeuvre description

To study the yaw stability of AHVs, all braking-in-turn manoeuvres presented in this section are simulated according to the following steps:

(1) The vehicle starts moving in a straight line with an initial longitudinal velocity of 40% of the considered speed limit V_x^{lim}. Unless otherwise stated, the friction coefficient of the road, μ, is equal to 0.3.
(2) After 20 m in a straight line and 10 m of transition, the vehicle enters a circular track. Unless otherwise stated, the turning radius is considered to be $R = 72$ m. A simple path-following algorithm based on the single-point preview method with a PID control is used as the driver model.

(3) Vehicle is accelerated up to V_x^{lim} by the propulsion torque applied at the drive axles of the tractor using a simple PID speed controller with a maximum friction utilisation of 40% and a maximum of 370 kW of power from the engine.
(4) When the longitudinal speed reaches V_x^{lim}, the speed controller is disabled and the engine torque is set to zero.
(5) After 0.5 seconds, the path follower is also disabled and the steering wheel angle is fixed for the rest of the manoeuvre.
(6) At the same time, the vehicle starts braking with forces of $c_{tractor} \cdot \mu \cdot F_z^{tractor,i}$ on the i^{th} drive-axle of the tractor ($i \in \{1, 2\}$) and $c_{trailer} \cdot \mu \cdot F_z^{trailer,j}$ on j^{th} axle of the semitrailer ($j \in \{1, 2\}$). Here, $F_z^{tractor,i}$ and $F_z^{trailer,j}$ are the normal load on the tractor's i^{th} drive axle and on the semitrailer's j^{th} axle. $c_{tractor}$ and $c_{trailer}$ are the friction utilisations. These are defined as negative for braking, and positive for propulsion. Unless otherwise stated, both drive axles of the tractor and/or both axles of the semitrailer are used for braking.
(7) The simulation is stopped if the articulation angle reaches $\pm 90^\circ$ (meaning that either severe jackknifing or trailer swing has occurred), or coming to a standstill.

2.2. Safety assessment criteria

A safe manoeuvre is defined according to the following criteria [11]:

$$\max(\Delta\beta_{1r}) < 5^\circ \quad \& \quad \max(\Delta\beta_2) < 3^\circ \tag{1}$$

where β_{1r} and β_2 are the respective axle side-slip angles for the centre of the drive axle group of the tractor and the semitrailer axle group. $\Delta\beta_{1r}$ and $\Delta\beta_2$, on the other hand, refer to the deviations of β_{1r} and β_2 with respect to their values at the time of brake force application (their quasi-steady-state values).

2.3. SOE derivation with VTM simulations

This section studies the yaw stability of a tractor-semitrailer combination vehicle. The specifications of the simulated vehicle are based on the real test vehicle specifications explained in Section 3.1. Many different combinations of braking forces for the tractor and semitrailer combination are simulated and associated SOEs are obtained.

All the simulations are performed by using a high-fidelity vehicle model (referred as the Volvo Transport Model or VTM) developed by Volvo Group Trucks Technology. The VTM library is a multi-body simulation tool used to simulate any combination of truck and trailer plants (developed with MATLAB®, Simulink®, Simspace™ Multibody™ and PAC2002 semi-empirical tyre model [28]) [29]. It is used for truck controller development, conceptual handling studies, driving simulators, crash reconstructions and functional safety analysis. The VTM library is validated with real tests and has proved sufficiently accurate for simulating the dynamical behaviour of any combination of truck and trailer [30,31]. All simulations include a slip controller that tries to limit longitudinal wheel slips to 10% during braking. However, this study does not use a stability controller. Mass, inertia, and length properties of the vehicle model are given in Table 1.

Simulations with many different combinations of longitudinal and lateral tyre forces are performed for a variety of tractor and semitrailer friction utilisations, $c_{tractor}$ and $c_{trailer}$, for

Table 1. Vehicle parameters used in VTM simulations.

Parameter Description	Value	Unit
Mass of the tractor	12,500	kg
Mass of the semitrailer	13,500	kg
Yaw moment of inertia of the tractor	48,758	$kg \cdot m^2$
Yaw moment of inertia of the semitrailer	83,913	$kg \cdot m^2$
Tractor wheelbase	4.085	m
Distance between coupling to the front axle of tractor	3.7725	m
Distance between the coupling to the semitrailer axle	7.05	m
Distance between the CoG and the front axle of tractor	1.534	m
Distance between the CoG and the semitrailer axle	1.9315	m

a selected longitudinal velocity set. This is done by varying $c_{tractor}$ and $c_{trailer}$ from 0 to -1 in steps of -0.1 (for braking), for various values of $V_x^{lim} \in [30, 35, 40, 45]$ km/h. Hence, a total of 484 simulations were conducted. A normalised lateral acceleration $c_y = \frac{a_y}{\mu \cdot g}$ can be defined, where a_y represents the lateral acceleration, g is the gravitational acceleration and μ is the friction coefficient [11]. In steady-state cornering, the lateral acceleration is determined as $a_y^{lim} = V_x^{lim^2} \cdot R^{-1}$. For the turning radius of $R = 72$ m and the longitudinal velocities of $V_x^{lim} \in [30, 35, 40, 45]$ km/h, the lateral accelerations are determined as follows: $a_y^{lim} \in [0.96, 1.31, 1.71, 2.17]\ m \cdot s^{-2}$. The normalised lateral accelerations are determined as $c_y \in [0.328, 0.446, 0.583, 0.737]$ for the selected set of longitudinal velocities and the friction coefficient of $\mu = 0.3$.

Figure 2 shows the maximum side-slip angle deviations for the tractor and semitrailer, $\max(\Delta\beta_{1r})$, $\max(\Delta\beta_2)$, and the maximum articulation angle deviation, $\max(\Delta\theta)$, for different tractor and semitrailer friction utilisations ($c_{tractor}$ and $c_{trailer}$) during braking at four different speeds. These maximum angle deviations are determined by comparing the corresponding quantity to its quasi-steady-state value, which is calculated at the moment the braking starts.

Although $\max(\Delta\theta)$ is also shown (in the third column) in Figure 2 as additional information, it is not considered part of the safety criteria presented in (1). This is because the articulation angle alone is not enough to capture the combination spin-out. The side-slip angles of the tractor and semitrailer are enough for detecting the occurrence of jackknifing, trailer swing and combination spin-out [11]. Articulation angle deviation could still serve as a complementary criterion, but is not used in this study.

In Figure 2, the braking scenarios leading to $\max(\Delta\beta_{1r})$ and $max(\Delta\theta)$ less than 5° and $\max(\Delta\beta_2)$ less than 3° are shown with green representing safe manoeuvres. Braking scenarios that exceed these limits are shown in yellow for moderately unsafe and red for highly unsafe scenarios.

At a velocity of 30 km/h ($a_y = 0.328 \cdot \mu \cdot g$), any combination of tractor and semitrailer braking, up to 100% friction utilisation, is safe and does not result in high side-slip angles or a high articulation angle. At 35 km/h ($a_y = 0.446 \cdot \mu \cdot g$), for full tractor braking with no semitrailer braking ($c_{tractor} = -1$, $c_{trailer} = 0$), jackknifing occurs. For full semitrailer braking ($c_{trailer} = -1$), no matter how much the tractor is braked, the semitrailer swings more than 3° and the manoeuvre becomes unsafe. The same observations are realised for a velocity of 40 km/h ($a_y = 0.583 \cdot \mu \cdot g$) but the unsafe regions grow larger. Thus, both full braking and braking with slightly less than full friction utilisation create similar problems.

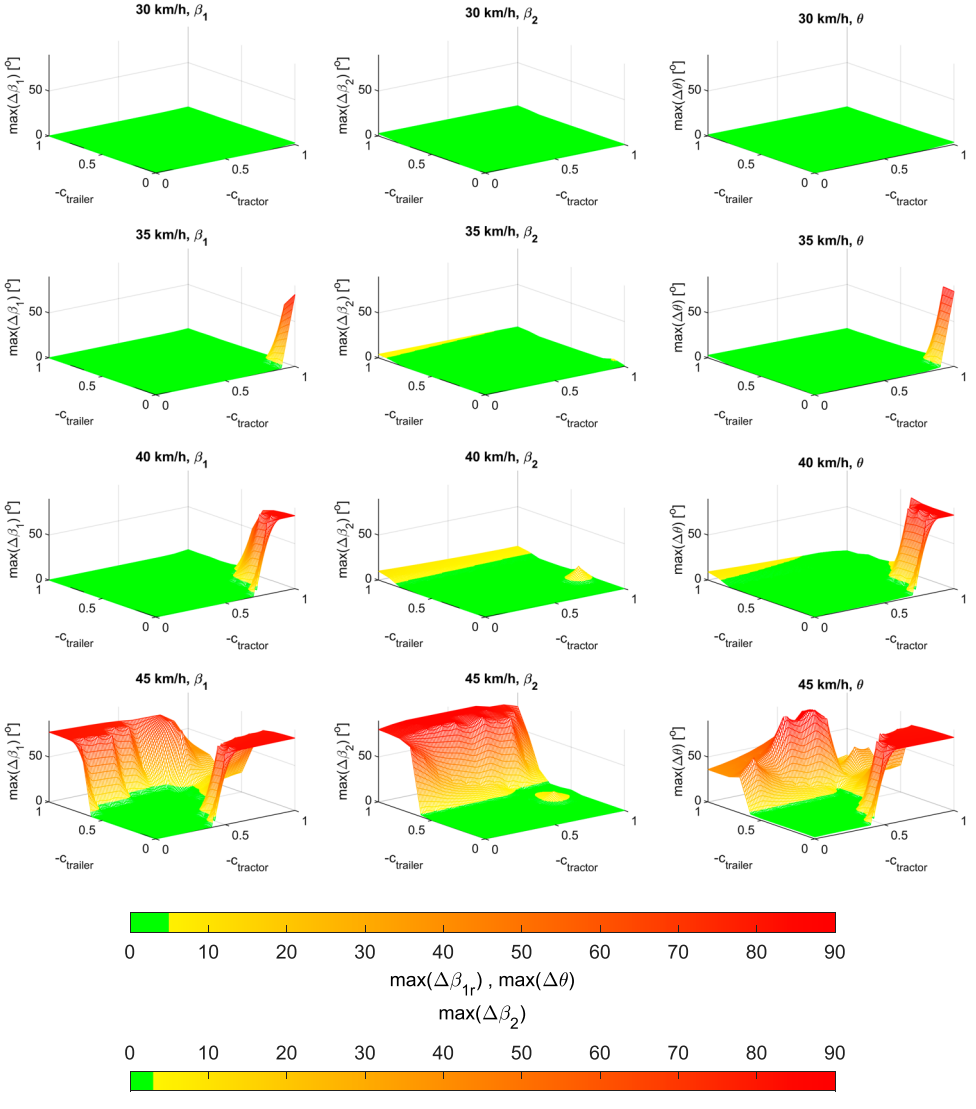

Figure 2. Maximum side-slip angle and articulation angle deviations for the braking scenarios with four different speeds obtained from VTM simulations.

The maximum achievable velocity of the vehicle driving in a circle of radius 72 m and a friction coefficient of 0.3 is about 45 km/h ($a_y = 0.737 \cdot \mu \cdot g$). Above this speed, the vehicle understeers and cannot keep its circular track. At this speed, trailer swing occurs due to the high degree of semitrailer braking. This increased semitrailer braking also leads to the tractor losing its lateral grip and swinging with the semitrailer. Trailer swing typically occurs regardless of how much the tractor is braked. For high degrees of tractor braking, on the other hand, jackknifing occurs. There again, if the semitrailer and tractor are braked together, jackknifing is more likely when there is a lower degree of semitrailer braking (for the same level of tractor braking). This shows that semitrailer braking can help avoid jackknifing as it results in stretch-braking.

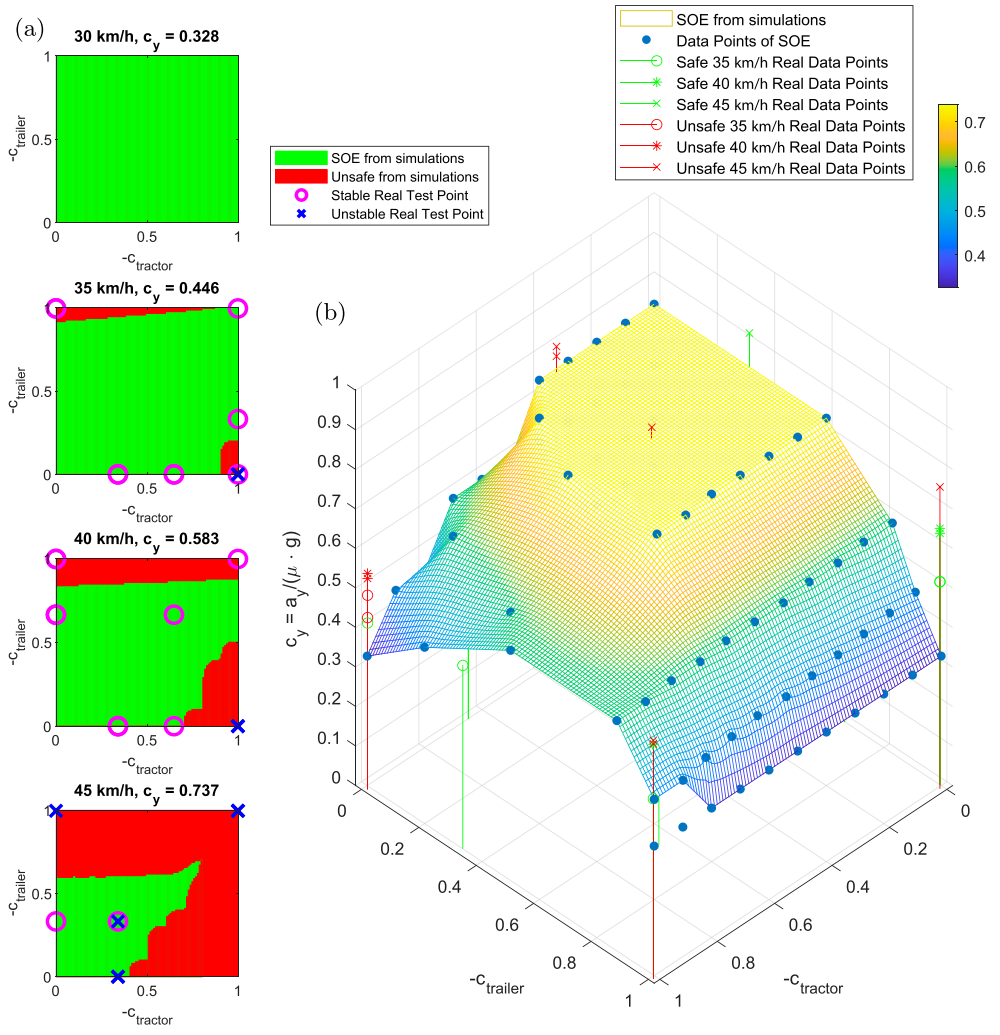

Figure 3. SOE obtained from the VTM simulations shown with real test data points.

Figure 3(a) illustrates SOEs obtained from VTM simulations for the braking of the tractor and semitrailer at four different longitudinal velocities (resulting in four different lateral accelerations). Safe combinations of the friction utilisations of the tractor and semitrailer ($c_{tractor}$ and $c_{trailer}$) are shown in green and unsafe combinations are depicted in red. The evaluation is based on the criteria provided in (1). The purple circles and blue crosses indicate the real test results, which will be explained in detail later in Section 3.4.

Figure 3(b) shows a three-dimensional SOE, which was obtained by interpolating the two-dimensional plots presented in Figure 3(a) for the intermediate values. Consequently, four plots from Figure 3(a) represent horizontal slices of the three-dimensional SOE shown in Figure 3(b), corresponding to four different c_y (which is the vertical axis). The vertical green and red stems represent the real test results, which will be explained later in Section 3.4.

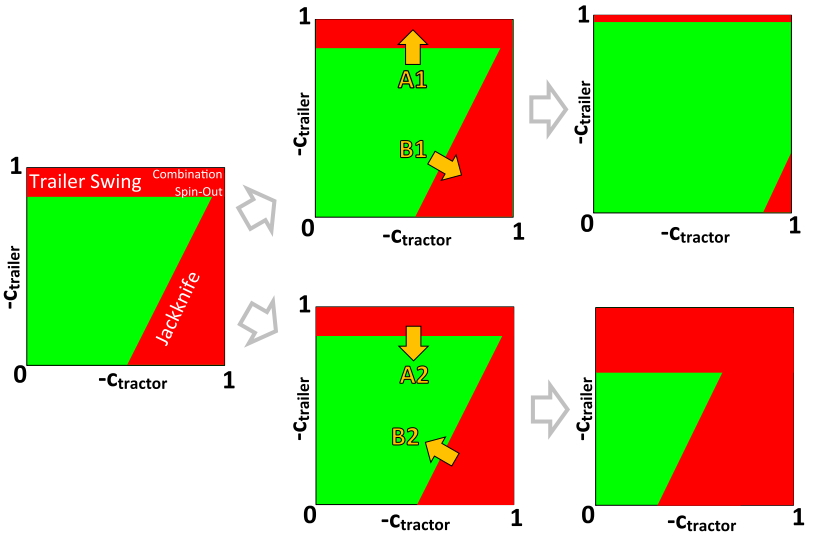

Figure 4. Four different form and size changes illustrated in a SOE.

All manoeuvres with combinations of lateral acceleration, tractor and semitrailer friction utilisations below the SOE shown in Figure 3(b) are safe manoeuvres, according to criteria given in (1). Likewise, all the manoeuvres with combinations of lateral acceleration, tractor and semitrailer friction utilisations above the SOE shown in Figure 3(b) are unsafe manoeuvres that lead to jackknifing, trailer swing or combination spin-out.

2.4. Sensitivity of SOE to parameter changes

SOEs obtained in Section 2.3 are valid only for a specific manoeuvre. For using SOE in a real application with AHVs, it is important to understand the sensitivity of SOE to parameter changes (such as friction coefficient, road slope, load distribution, and so on). In this section, the effects of different vehicle and environmental parameters on the SOEs are investigated.

For ease of explanation, Figure 4 shows four main size changes on the SOE. The first column of Figure 4 gives an instance of an SOE. Typically, SOE is below (in the absolute sense) a certain semitrailer friction utilisation ($c_{trailer}$) and this limit does not change significantly as a function of tractor utilisation ($c_{tractor}$). Hence, the SOE is bounded by an almost horizontal line (rather parallel to the x-axis, where the x-axis represents $c_{tractor}$ and the y-axis represents $c_{trailer}$) from the top. The red area above this line is typically where the trailer swing occurs. However, with respect to tractor friction utilisation $c_{tractor}$, the SOE is not limited by a perpendicular line (parallel to the y-axis) but rather by a positively inclined line. Hence, the tractor can brake more without instability if the semitrailer is also braking.

The triangular red area in the bottom right-hand corner typically corresponds to where the jackknifing occurs. Finally, a combination spin-out occurs, typically as a continuation of jackknifing or trailer swing or it may occur when both units lose lateral grip at the same time. This is typical when the friction utilisations of both units are high (in the absolute sense), where this situation is observed in upper right-hand corner of the SOE plots.

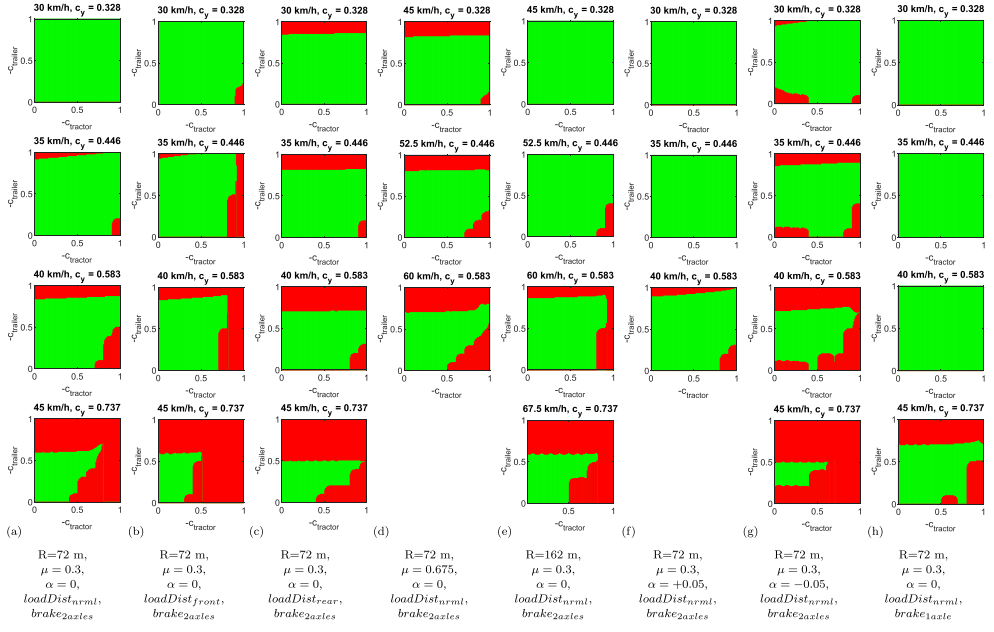

Figure 5. SOEs for 4 different normalised lateral accelerations for the base case (a), different load distributions (b,c), friction coefficient (d), turning radius (e), slopes (f,g), number of axles used for braking (h).

Table 2. Axle loads for 3 different load cases.

	Load Case	Axle 1 [tons]	Axle 2 [tons]	Axle 3 [tons]
Tractor	$loadDist_{nrml}$	6.69	3.63	3.63
	$loadDist_{front}$	7.15	6.43	6.43
	$loadDist_{rear}$	6.57	2.92	2.92
Semi trailer	$loadDist_{nrml}$	4.90	4.90	0
	$loadDist_{front}$	4.37	4.37	0
	$loadDist_{rear}$	8.17	8.17	0

Contraction of the trailer swing area is designated A1 and expansion of the trailer swing area is designated A2, as shown in the second column of Figure 4. Similarly, the contraction of the jackknifing area is designated B1 and the expansion of the jackknifing area is designated B2, as shown in the second column of Figure 4. The new SOE instances after the expansion or contraction are shown in the third column of Figure 4.

Figure 5 displays the SOEs of four different c_y, for different vehicle and environmental parameters. Figure 5(a) shows the base case with a 72 m turning radius, 0.3 friction coefficient, 0 road slope, the base load distribution (load case $loadDist_{nrml}$, explained in Section 3.1), and braking with two tractor drive axles and/or two semitrailer axles. Figure 5(b) depicts SOEs for the same vehicle with an additional five tons payload and the payload centre of gravity shifted forwards by 3 m (load case $loadDist_{front}$). Figure 5(c) presents SOEs for the same vehicle, but with an extra five tons payload and the payload centre of gravity shifted backwards by 3 m (load case $loadDist_{rear}$). Axle load distributions for these three loading cases are provided in Table 2.

The $loadDist_{front}$ case has relatively similar semitrailer axle loads to $loadDist_{nrml}$ and significantly higher tractor drive axle loads. $loadDist_{rear}$ case, on the other hand, has fairly similar tractor axle loads to $loadDist_{nrml}$ and significantly higher semitrailer axle loads. Hence, with these three load cases, it is possible to see the effects of increased axle loads on the braking axles. According to the SOEs shown in Figure 5(b), increasing the drive axle loads of the tractor changes the envelope in the B2 direction. Hence, the probability of jackknifing increases for the same friction utilisation, yet the probability of trailer swing doesn't change significantly. According to the SOEs shown in Figure 5(c), increasing the semitrailer axle loads changes the envelope in the A2 direction. Thus, the probability of trailer swing increases for the same friction utilisation, but the probability of jackknifing doesn't change significantly.

Figure 5(d) displays the SOEs obtained with a friction coefficient that is 2.25 times greater ($\mu = 0.675$) and longitudinal speeds 1.5 times greater than the base case (resulting in the same c_y), while all other vehicle and environmental parameters are kept the same as the base case. Because the simulated AHV was unable to reach the 67.5 km/h longitudinal speed corresponding to $c_y = 0.737$ in a quasi-steady state, it was not possible to obtain the last plot for $c_y = 0.737$ and so this is kept empty. A comparison of the plots given in Figure 5(a,d) shows that if the same c_y is obtained using a greater longitudinal speed and higher friction coefficient, the SOE gets smaller due to a contraction in both A2 and B2 directions (see Figure 4).

Figure 5(e) illustrates SOEs obtained with a 2.25 times larger turning radius and 1.5 times greater longitudinal speeds than the base case (resulting in the same c_y), while all other vehicle and environmental parameters are kept the same as the base case. The comparison of plots in Figure 5(a,e) does not show a significant trend for the SOE size change and exhibits none of the significant A1, A2, B1 and B2 changes shown in Figure 4. Indeed, the SOEs presented in Figure 5(a,e) are somewhat similar (albeit with minor differences). Hence, if the same normalised lateral acceleration is obtained with a greater longitudinal speed and larger turning radius, the SOE stays almost the same.

Figure 5(f,g) illustrate SOEs for the uphill slope of $\alpha = +0.05$ and downhill slope of $\alpha = -0.05$ respectively, while all other vehicle and environmental parameters are kept the same as the base case. It is important to note that for the uphill slope of $\alpha = +0.05$, the simulated AHV was unable to reach the 45 km/h longitudinal speed corresponding to $c_y = 0.737$ in a quasi-steady state manner. As a result, the last plot for $c_y = 0.737$ in Figure 5(f) could not be generated and is kept empty.

A comparison of the plots provided in Figures 5(a,f) shows that the SOE for the uphill slope expands in both A1 and B1 directions, as illustrated in Figure 4. Similarly, comparing the plots in Figure 5(a,g) reveals that the SOE for the downhill slope shrinks due to contractions in both the A2 and B2 directions, as depicted in Figure 4. The contraction of the SOE at the lower left corner of Figure 5(g), corresponding to low (in the absolute sense) $c_{tractor}$ and $c_{trailer}$ coefficients, on the other hand, is because the AHV has not been braked sufficiently. Its longitudinal speed increases due to the downhill slope, eventually leading to jackknifing or trailer swing. Hence, this contraction is trivial and irrelevant in this context.

Lastly, in Figure 5(h), SOEs are presented for scenarios when braking is performed using only a single axle of the AHV, while keeping all other vehicle and environmental parameters identical with the base case. A comparison of plots given in Figures 5(a,h) shows that the SOE for single-axle braking expands in both A1 and B1 directions, as shown in Figure 4.

Indeed, yaw instabilities only occur at very high c_y, while no yaw instabilities are observed at smaller lateral accelerations. This shows that, if only one axle is electrified out of two or three tractor rear axles or semitrailer axles, AHVs can fully and safely utilise the friction for regenerative braking, except in the case of very large c_y.

At first glance, the red (indicating instability and jackknifing) area at ($c_{tractor} = -0.6, c_{trailer} = 0$) in the fourth plot seems to be an outlier. This point is where the inner wheel starts to have slip controller activation. The outer wheel, on the other hand, does not have slip controller activation because the load transfer makes the outer wheel experience a larger normal load. Thus, the same amount of braking force corresponds to a smaller friction utilisation at the outer wheel. For the two cases of ($c_{tractor} = -0.6, c_{trailer} = 0$) and ($c_{tractor} = -0.7, c_{trailer} = 0$), although the inner wheels have a somewhat similar braking force (due to brake force saturation caused by slip controller activation), the braking force of the outer wheel is higher for the second case ($c_{tractor} = -0.7, c_{trailer} = 0$). This means that the AHV experiences large lateral acceleration for a shorter duration. The saturation of the tyre forces is also shorter-lived due to a faster decrease in lateral tyre forces (caused by a quicker drop in lateral acceleration). Hence, although the braking force is higher, jackknifing does not occur. This is unlike the first case ($c_{tractor} = -0.6, c_{trailer} = 0$), in which jackknifing does occur. In short, this exceptionally unstable point aligns with the overall conclusion drawn so far and does not contradict them.

3. Validation of SOE with real tests

This section compares the SOE obtained from simulations (as discussed in Section 2.3) with the test results obtained from a real vehicle.

3.1. Test vehicle specifications

The test vehicle, as depicted in Figure 6, consists of two vehicle units: a 6x4 Volvo FH16 and a semitrailer equipped with three liftable axles. The semitrailer is consistently tested with the two frontmost axles lowered and the rearmost axle lifted. The reason for lifting the third axle of the semitrailer is to create a fairer comparison of tractor and semitrailer actuator forces, by applying forces on two axles per unit. The semitrailer is loaded with an extra 5 tons payload. The static normal load on the front axle of the tractor is 6.7 tons and the normal load on the drive axles is 3.6 tons per axle. For the semitrailer, the normal load on the first two axles is 4.9 tons per axle, with the third axle lifted. Hence, the total weight of the tractor and semitrailer is 23.7 tons.

Both tractor and semitrailer are equipped with highly accurate OxTS RT3000 GNSS/INS (Global Navigation Satellite System/Inertial Navigation System) [32] for measuring the vehicle motion states such as acceleration, angular rates, side-slip angles, and global position. Additionally, the semitrailer is equipped with an articulation angle sensor and the fifth wheel of the tractor is equipped with a load cell for measuring the longitudinal coupling force.

All the signals are logged using the Dewesoft® Sirius® data acquisition system [33] via CAN interface. Additionally, all the control commands are sent to the advanced engineering interfaces of the tractor's or semitrailer's EBS modules via a dSPACE MicroAutoBox II [34].

The tractor frame is reinforced with sheet steel, and the semitrailer is connected to the reinforced tractor frame using the steel cables depicted in Figure 7. These steel cables are loose during normal driving conditions. However, when the articulation angle grows up to $\pm 60^{\circ}$, the cables are stretched preventing a catastrophic jackknifing or trailer swing. Throughout all tests, the electronic stability controller is turned off, while the anti-lock braking system remains active.

3.2. Test track specifications

All the tests were performed on the circular ice tracks at the Hornavan lake (Colmis Test Facility, Arjeplog, Sweden) shown in Figure 8. The inner radius of the track is 50 m, and the outer radius is 80 m.

The surface friction coefficient at the test track was measured with two different tests: full braking with all axles in a straight line, and driving the vehicle at the highest speed possible in a circle. Although the average friction coefficient observed was 0.3 (typical for packed snow), the friction on different parts of the track was heterogeneous. This means that as more tests are performed on the same spot, the friction coefficient at that particular point decreases due to the snow melting because of the pressure applied by the vehicle and then re-freezing.

Figure 6. Tractor and semitrailer test vehicle.

Figure 7. Jackknifing protection cables shown under the semitrailer.

Figure 8. Circular track on the Hornavan lake, Colmis Test Facility, Arjeplog, Sweden [35].

3.3. Manoeuvre description

All the tests were performed with a human driver, as follows:

(1) The driver starts driving from a standstill on a path with a turning radius of 70 ± 5 m, depending on the test. Driving the vehicle on a path with a similar turning radius for each test means that the lateral accelerations obtained, a_y, are close to each other (but not precisely equal) for the tests performed with the same longitudinal speed.
(2) The driver accelerates the vehicle to a speed that is 1 or 2 km/h more than the set speed V_x^{lim}.
(3) The driver stops pressing the accelerator pedal and selects neutral gear.
(4) The vehicle starts to slow down due to resistive forces.
(5) Once the vehicle slows down to the set speed V_x^{lim}, an automatic braking request is sent to the selected axles of the vehicle via MicroAutobox II.
(6) The vehicle begins to slow down. The driver is still responsible for keeping the steering wheel angle the same. However, the driver doesn't try to save the vehicle by, say, counter-steering during a jackknife. Three possible scenarios may arise:
    (a) (a)The vehicle slows down to a standstill with no significant yaw instability, such as jackknifing or trailer swing.
    (b) (b)The vehicle slows down to a standstill while exhibiting jackknifing or trailer swing. However, since the vehicle is unlikely to reach the limits of the track, the driver doesn't take control and just keeps the steering wheel angle the same. The brake test continues until a standstill is reached.
    (c) (c)The vehicle begins to slow down but exhibits a highly unsafe jackknifing or trailer swing that causes the vehicle to reach the limits of the track and potentially hit the snow piles at the sides. In this case, the automatic braking request is stopped and the driver takes control of the vehicle and tries to save it. The driver either saves the vehicle from hitting the snow piles at the side or the vehicle hits them. In the case of aggressive jackknifing or trailer swing, the articulation angle may reach $\pm 60^\circ$, and the anti-jackknifing cables may prevent the cab from hitting the semitrailer.

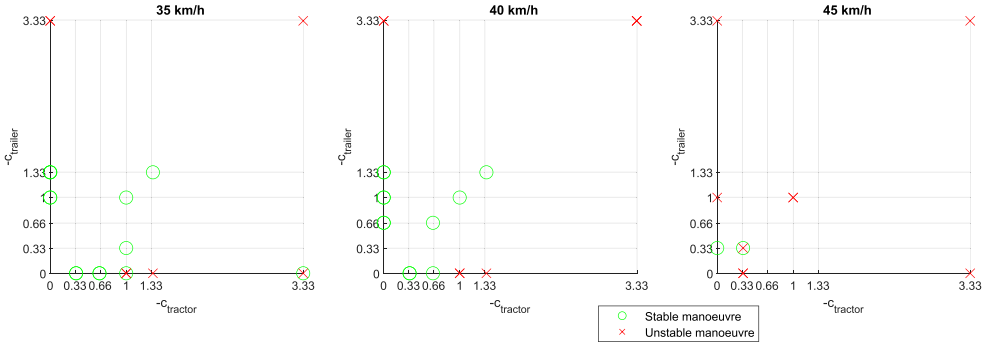

Figure 9. Yaw stability test results for different braking scenarios performed on the real vehicle.

3.4. Test results

This section presents the results of real braking tests and compares them to the SOE obtained in Section 2.3. Figure 9 displays 52 real tests performed at three different speeds (35 km/h, 40 km/h, 45 km/h). Stable manoeuvres are indicated by green circles and unstable manoeuvres are marked by red crosses, based on the criteria provided in (1). Table 3 presents the maximum side-slip angle deviations and their corresponding normalised lateral acceleration c_y for each real test and VTM test. The maximum side-slip angle deviations violating the safety criteria are highlighted in red, while the safe ones are indicated in green.

Friction utilisations for the tractor and semitrailer, ($c_{tractor}$ and $c_{trailer}$), as tested with a real test vehicle, are as follows: [0, −0.33, −0.66, −1.00, −1.33, −3.33]. Normally, −1.00 represents the largest friction utilisation (in the absolute sense) that can be reached during braking. Hence, testing values like −1.33 and −3.33 may seem redundant. However, there are three reasons to test friction coefficients greater than 1 (in the absolute sense) as listed below:

(1) Although, the friction coefficient is found to be 0.3, the friction is also observably quite heterogeneous. In particular, after performing many tests on the same spot, the friction coefficient is observed to be decreasing over time (down to, say, 0.1). Similarly, untested areas with more fresh snow may be observed to have a greater friction coefficient (such as 0.4). Requested friction utilisations ($c_{tractor}$ and $c_{trailer}$), [0, −0.33, −0.66, −1.00, −1.33, −3.33] always assume the friction coefficient to be $\mu = 0.3$, meaning that the requested brake force is calculated by multiplying the requested friction utilisation with normal load and a friction coefficient of 0.3. However, for $\mu = 0.4$, for example, the requested friction utilisations of −1.00 and −1.33 result in realised friction utilisations of −0.75 and −1.00, respectively. If the friction coefficient is, say, 0.45, the requested friction utilisation of −1.33 results in a realised friction utilisation of −0.89. So, for a friction coefficient greater than 0.4, even the requested friction utilisation of −1.33 results in a realised friction utilisation of less than full friction utilisation. To cover full friction utilisation for every heterogeneous friction area with greater friction than $\mu = 0.3$ at the test track, friction utilisations of −1.33 and −3.33 are also included in the test points.

(2) All the $c_{tractor}$ and $c_{trailer}$ values listed so far in this study are requested values but not the real friction utilisation status. Slip controller performance (anti-lock braking system, ABS, for braking) is a very important factor when it comes to yaw instabilities. If the slip controller performs well and keeps the slips to a good level so that there is enough lateral capability, even though full friction utilisation ($c_{tractor} = \pm 1$ and/or $c_{trailer} = \pm 1$) is requested, the obtained friction utilisation would be less (in the absolute sense) and no yaw instability may occur. However, if the slip controller performance is bad, then yaw instability may occur. Hence, in real tests, friction utilisations greater than 1 (in the absolute sense) are also tested to push the limits of the slip controller. As the request is higher, the applied brake pressure until the slip controller gets activated would be greater and a greater drop at the wheel speeds can be observed, meaning that the slip rises to a higher value instantaneously, for -1.33 and -3.33 friction utilisation requests, compared to -1.00. Thus, it is possible to test for poorer slip control performance.

(3) Tested friction utilisations are calculated with static load distribution. However, there may be significant lateral load transfer due to high lateral accelerations. For example,

Table 3. Side-slip angle deviations obtained at real tests, and VTM model.

C trailer	max (Δβ1r) [°]	max (Δβ2) [°]	Cy	C tractor = 0	C tractor = -0.33	C tractor = -0.66	C tractor = -1	C tractor = -1.33	C tractor = -3.33	
... C trailer = -3.33	0	4.3	0.47						1.9	Test 1
	0	6.7	0.51						5.2	Test 2
									0.4	Test 3
	0	13.3	0.43	0	12.3	0.43	0	11.3	0.43	0.8	11.1	0.43	2	11.8	0.43	23.4	13.3	0.43	VTM
C trailer = -1.33	0	0.3	0.48						1	0.5	0.45				Test 1
	0	1.6	0.53												Test 2
	0	0.5	0.48												Test 3
	0	5.7	0.43	0	5.2	0.43	0	4.8	0.43	0.9	4.3	0.43	2.2	3.9	0.43	16	7.6	0.43	VTM
C trailer = -1	0	0.3	0.51				0.7	0.1	0.44						Test 1
	0	0.2	0.51												Test 2
															Test 3
	0	3.9	0.43	0	3.6	0.43	0	3.2	0.43	0.9	2.7	0.43	2.2	3	0.43	15.6	6.6	0.43	VTM
C trailer = -0.66															Test 1
															Test 2
															Test 3
	0	0	0.43	0	0	0.43	0	0	0.43	1	0	0.43	2.4	0.2	0.43	13.7	5.2	0.43	VTM
C trailer = -0.33							2.1	0	0.46						Test 1
															Test 2
															Test 3
	0	0	0.43	0	0	0.43	0	0	0.43	1.7	0.1	0.43	3.7	0.9	0.43	75.6	0.8	0.43	VTM
C trailer = 0				0.2	0	0.44	0.8	0	0.50	3.8	0	0.41	44.3	7.1	0.40	4.8	0.4	0.30	Test 1
				0.1	0	0.46	0.6	0	0.49	48	18.7	0.49				45.7	10.1	0.29	Test 2
										44.1	10.3	0.43							Test 3
	0	0	0.43	0	0	0.43	0.3	0	0.43	80.1	0.9	0.43	80.7	0.7	0.43	81.4	0.3	0.43	VTM

(a) Results for 35 km/h longitudinal speed

(*continued*).

a request of $c_{tractor} = -1$ may become $c_{tractor} = -0.9$ for the outer wheel due to an increase in normal load, and $c_{tractor} = -1.1$ for the inner wheel due to decrease in normal load. Hence, to cover full friction utilisation for the outer wheel, something greater (in the absolute sense) than $c_{tractor} = -1$ should be tested.

Many of the test points shown in Figure 9 are tested multiple times. When the results from different tests are not the same, then both a red cross and a green circle are shown at the respective test point. The first reason for obtaining different results for the same test point is due to the heterogeneous friction, as previously explained. So, even when the test speeds and friction utilisations ($c_{tractor}$ and $c_{trailer}$) remain the same, the friction coefficient may be different between the tests. Another contributing factor is the human driver; the turning radii in the real tests are not consistently maintained at precisely 72 m for each test. Rather, the turning radii vary from 70 ± 5 m depending on the test. This leads to different normalised lateral accelerations c_y for the same speeds, unlike the simulations which have the same c_y for the same speeds. However, it is important to note that the speeds at which the braking starts (35 km/h, 40 km/h and 45 km/h) are precise for each test. This is because

Table 3. Continued.

C trailer	max (Δβ1r) [°]	max (Δβ2) [°]	Cy	C tractor = 0	C tractor = -0.33	C tractor = -0.66	C tractor = -1	C tractor = -1.33	C tractor = -3.33	
... C trailer = -3.33	0	8.8	0.64						34.4	Test 1
	0	16.7	0.63						64.5	Test 1
									4.6	Test 2
									18.8	Test 2
									5.5	Test 3
									21.5	Test 3
	0.6	46.4	0.55	0	37.2	0	32.3	1.6	62.9	0.55	67.1	79.4	0.55	74.5	22.2	0.55	VTM
C trailer = -1.33	0	0.9	0.65								1.9	0.3	0.56				Test 1
	0	1	0.50														Test 2
																	Test 3
	0	16.2	0.55	0	13.4	0.55	0	11.4	0.55	2.3	13.6	0.55	33.9	16.5	0.55	35.3	11.8	0.55	VTM
C trailer = -1	0	0.1	0.65							1.5	0.2	0.58							Test 1
	0.1	2	0.64																Test 2
																			Test 3
	0	9.9	0.55	0	8	0.55	0	6.6	0.55	2.2	6	0.55	15.7	6.7	0.55	33.4	10.1	0.55	VTM
C trailer = -0.66	0	0	0.60			0.1	0	0.6											Test 1
	0	0.1	0.61																Test 2
																			Test 3
	0	0	0.55	0	0	0.55	0	0	0.55	1.8	0	0.55	7.8	2	0.55	28.8	6	0.55	VTM
C trailer = -0.33																			Test 1
																			Test 2
																			Test 3
	0	0	0.55	0	0	0.55	0.1	0	0.55	71.8	0.2	0.55	75	0	0.55	79.2	0	0.55	VTM
C trailer = 0				0.1	0	0.62	0.7	0	0.54	48.8	8.1	0.53	49.7	8.4	0.53				Test 1
				0.2	0	0.55				47.5	7.8	0.55							Test 2
																			Test 3
	0	0	0.55	0.1	0	0.55	0.7	0	0.55	81.2	0	0.55	81.5	0	0.55	81.8	0	0.55	VTM

(b) Results for 40 km/h longitudinal speed

(*continued*).

Table 3. Continued.

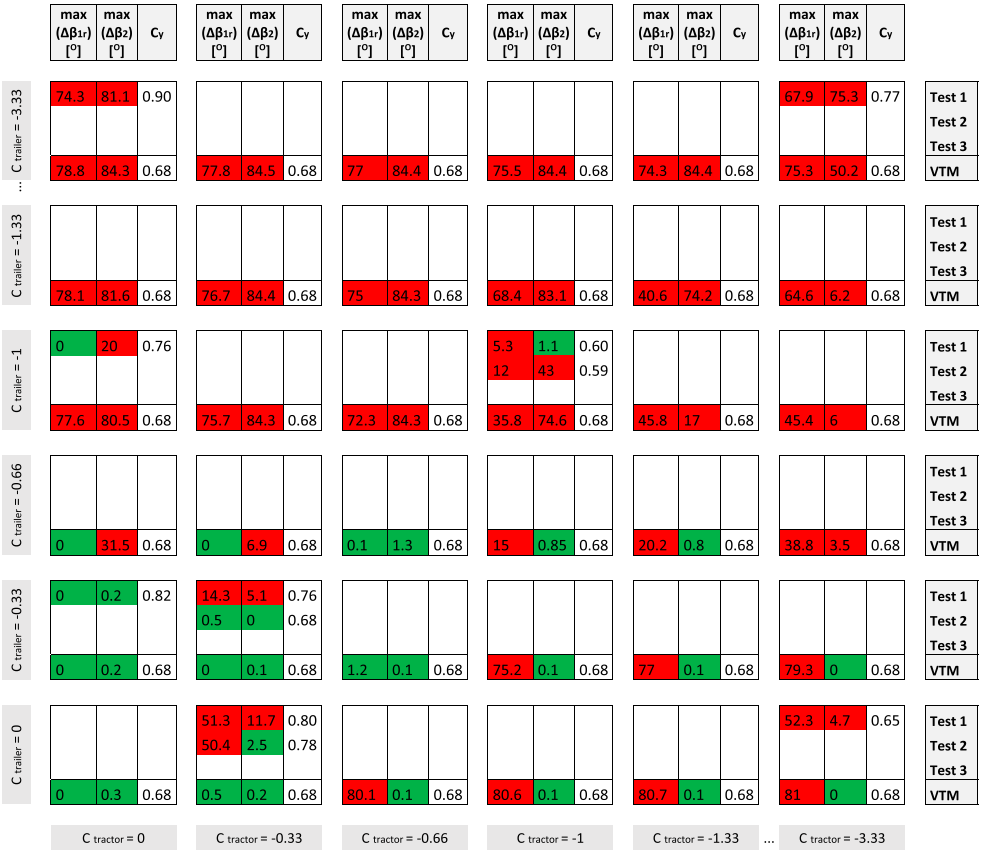

(c) Results for 45 km/h longitudinal speed

the braking is done automatically at the set speeds and with similar brake force requests (thus similar friction utilisation requests $c_{tractor}$ and $c_{trailer}$, but calculated with respect to static axle loads). Another reason for obtaining different results at the same test point is that the instantaneous distribution of axle loads may differ, as the electronically controlled air suspension system may slightly change the axle loads over time.

The real test results presented in Figure 9 are generally in agreement with the VTM simulation results discussed in Section 2.3. In Figure 3, both the real test results and VTM results are presented within the same plots. Note that, as previously explained, the real test results in each subplot have precisely matching set speeds (35 km/h, 40 km/h, 45 km/h), although they may have slightly different c_y values.

In the 35 km/h plot displayed in Figure 3(a), the VTM and real test results are generally a good match. When considering the test with $c_{tractor} = 0, c_{trailer} = -1$, the VTM simulation performs unstable manoeuvre, while the real test remains stable. However, when the semi-trailer is braked more ($c_{tractor} = 0$, $c_{trailer} = -3.33$), the real test also becomes unstable. For both real tests, $c_{trailer} = -1.00$) and $c_{trailer} = -3.33$), the slip controller is activated, but the latter one has poorer slip control performance, leading to the semitrailer swinging. However, in the first one ($c_{trailer} = -1.00$) the slip controller is successful enough to

leave enough lateral tyre force capability to avoid trailer swing. Therefore, this unmatching between the real and simulation test results can be attributed to variations in slip control performance. Another unmatching result for 35 km/h is one of the ($c_{tractor} = -1$, $c_{trailer} = 0$) tests, which shows that, unlike the VTM results, it is a stable manoeuvre. However, the data from the two other real tests is in agreement with the VTM result. Checking the corresponding c_y values from Table 3 shows that the stable real manoeuvre actually has $c_y = 0.41$, which is less than the other two real tests (0.49 and 0.43) and the VTM simulation (0.43), as explained above. For the real tests with higher c_y values (0.49 and 0.43), the results align with the VTM simulations for that specific point ($c_{tractor} = -1$, $c_{trailer} = 0$). Therefore, the unmatching results arise due to the lower lateral acceleration observed in the real test.

For the 40 km/h plot shown in Figure 3(a), there is a general alignment between the VTM and real test results. All the points, except those corresponding to full friction utilisations for the semitrailer, namely ($c_{tractor} = 0$, $c_{trailer} = -1$) and ($c_{tractor} = -1$, $c_{trailer} = -1$), show agreement. For greater brake force requests, in other words for ($c_{tractor} = 0$, $c_{trailer} = -3.33$) and ($c_{tractor} = -3.33$, $c_{trailer} = -3.33$), which result in poorer slip control performance, real test manoeuvres also become unstable and match the VTM results. Thus, the reason for the unmatching results (similar to those observed at 35 km/h) is better slip control performance in the real tests, allowing for larger lateral force capability.

Lastly, in the 45 km/h plot depicted in Figure 3(a), the VTM and real test results are in agreement, except for two tests, ($c_{tractor} = -0.33$, $c_{trailer} = -0.33$) and ($c_{tractor} = -0.33$, $c_{trailer} = 0.00$). However, by checking Table 3, it is possible to see that both tests performed for ($c_{tractor} = -0.33$, $c_{trailer} = 0.00$) have a much higher c_y (0.80 and 0.78) compared to c_y of the VTM simulation which is 0.68. Similarly, the unsafe manoeuvre in the real tests for ($c_{tractor} = -0.33$, $c_{trailer} = -0.33$) has much a higher c_y (0.76) compared to c_y of VTM simulation which is 0.68. On the other hand, the other manoeuvre from the real tests, which resulted in a safe manoeuvre for the same point ($c_{tractor} = -0.33$, $c_{trailer} = -0.33$) has $c_y = 0.68$ which matches the c_y value of the VTM simulation. Hence, the reason for the discrepancy between the real and simulation results can be attributed to the higher lateral acceleration observed in the real tests compared to VTM simulations. This shows the need to introduce the lateral acceleration as an extra dimension in the SOE for a fairer comparison.

In Figure 3(b), a three-dimensional SOE surface obtained from VTM simulations is presented alongside with stem plots representing the real test data. Safe real test data points are shown in green, while unsafe real data points are indicated in red. In this plot, real test data is plotted with the corresponding normalised lateral acceleration c_y values (in the vertical axis). Consequently, due to previously mentioned factors, even for the same test speeds the vertical coordinate of the test points (c_y) may be different. The comparison of the real test results and simulation results in the previous paragraphs was done by mainly referring to plots in Figure 3(a). However, a comparison considering Figure 3(b) is fairer since the previously mentioned lateral acceleration differences even in the same test speeds can be truly reflected in the plot thanks to the vertical axis (c_y).

As shown in Figure 3(b), all the real test points below the three-dimensional SOE obtained from the VTM simulations are identified as safe, based on the criteria given in (1). This validation indicates that no real tests within the SOE had a yaw stability problem. However, there are some real test points above the SOE that are also identified as safe, but

the majority of the real test points located outside the SOE are identified as unsafe. This suggests that the SOEs obtained from the VTM simulations may be rather over-safe.

4. Conclusions

In this paper, first, safe operating envelopes (SOEs) for a tractor-semitrailer vehicle combination were obtained by using the Volvo Transport Model (VTM) multi-body simulation tool. These SOEs were specifically focussed on braking-in-curve scenarios. Next, the effects of various vehicle and environmental parameters on these SOEs were investigated. Lastly, the SOEs derived from VTM simulations were validated by comparing them to real test data.

As explained in the introduction, SOEs can be computed offline for various parameters, such as different load distributions and friction levels. These precomputed SOEs can then be stored in the vehicles' memory. An alternative approach to simulating all possible cases would be to simulate some base cases and expand or contract the SOE by a predetermined amount as needed to account for parameter changes. For instance, the base case shown in Figure 3 can be simulated offline and saved in the AHV's memory. Then, online adjustments can be made to accommodate changes in parameters such as road slope, load distribution, allowing instantaneous expansion or contraction of the stored SOE. The impact of those parameters on the SOE was explained in Section 2.4. More simulations can be performed to explore the effects of combinations of parameter changes, such as variations in friction and turning radii together.

As an alternative to considering the effects of changes in various parameters on the SOE, the combination of parameters corresponding to the smallest SOE can be used. Hence, the smallest possible SOE can be used for all cases to prioritise safety and deal with uncertain parameters. Alternatively, the VTM model can be simplified (with, say, lumped axles or a simpler tyre model) to decrease its computational cost and then run online in the real AHV.

The SOE obtained from the VTM simulations can be shrunk by applying a safety factor, for example, 30%, to account for model and parameter uncertainties. This safety factor can be increased, say, by 50%, for scenarios involving higher lateral accelerations. The SOE corresponding to the instantaneous operating conditions, such as speed, and turning radius, of the AHV should be instantaneously utilised. After changing the operating point, such as increasing or decreasing speed or turning radius, an updated SOE corresponding to the new operating conditions should be employed. Hence, the SOE is a function of multiple operating parameters.

The SOE presented in this paper, which was obtained using a VTM model, was validated using real test data and proved to be safe. This means that all points tested within the SOE using a real AHV were identified as safe. Indeed, the SOE derived from VTM is over-safe and conservative, meaning that some real test points outside of the SOE were also identified as safe. Achieving a highly accurate SOE from the simulations is challenging due to parameter and modelling inaccuracies. More specifically, modelling stochastic real-world parameters like friction will always be a challenge [36] and that explains some of the inconsistencies. Nevertheless, as long as it is shown that all points inside the SOE, obtained through deterministic simulations, are safe in the real tests involving stochastic parameters like friction, the SOE obtained from simulations remains a reliable reference

for use in real vehicles. Additionally, stochastic parameter behaviours can be included in the simulations to reflect the real world parameters in a more accurate way.

One of the biggest modelling challenges involves the slip controller, which can be improved to better align with the real data. Additionally, cornering stiffness and other parameters of the real tyres can be detected with some characterisation tests and more accurate tyre data can be used. Improving the accuracy of hard-to-obtain parameters, such as centre of gravity, can enhance the fidelity of simulations to match better with real vehicle performance. For instance, the centre of gravity height is an important parameter that significantly influences lateral load transfer, particularly under conditions of higher lateral acceleration.

The SOEs obtained from the VTM simulations and validated with real tests can be used to validate the SOEs obtained from the nonlinear single-track model presented in [11]. After validating the simpler model with VTM simulations, this simpler model (which is computationally more efficient) can be used to obtain SOEs online in a real AHV. Alternatively, weak and inaccurate points can be identified in the simpler models and the simpler models can still be used whilst taking the weaknesses into consideration. As an example, SOEs obtained from simpler models can be used with some safety factors (such as decreasing the size of SOE by 30%), or the SOE can only be used under certain circumstances (such as only for the lower lateral accelerations).

This study primarily focuses on analysing the yaw stability of AHVs. However, it is important to note that rollover is another critical safety aspect for AHVs, and there is potential to incorporate the rollover constraints into the SOE. The inclusion of the rollover envelope would result in modifying the SOE by cutting along a surface to exclude the higher lateral accelerations.

In future research, the integration of the SOEs obtained from the VTM simulations into a control algorithm and testing with a broader range of manoeuvres, including those beyond the scope of this paper (e.g. sine with dwell or lane change manoeuvres) could be explored. These evaluations should be performed in both simulations and real vehicle testing to evaluate potential benefits of the SOEs.

It is anticipated that the SOEs will contribute to improved safety and the mitigation of yaw instabilities in AHVs. This study represents a promising direction for future research aimed at enhancing AHVs safety and stability.

Disclosure statement

No potential conflict of interest was reported by the author(s).

Funding

This work was supported by VINNOVA [VINNOVA / FFI 2020-05144].

ORCID

Umur Erdinc http://orcid.org/0000-0001-5143-7104
Mats Jonasson http://orcid.org/0000-0002-7385-5195
Maliheh Sadeghi Kati http://orcid.org/0000-0003-3079-4801
Bengt Jacobson http://orcid.org/0000-0002-5798-5651
Jonas Fredriksson http://orcid.org/0000-0002-9814-6416
Leo Laine http://orcid.org/0000-0002-0672-3985

References

[1] Bienkowski BN, Walton CM. The economic efficiency of allowing longer combination vehicles in Texas. Center for Transportation Research, The University of Texas at Austin; 2011. (Research report, SWUTC/11/476660-00077-1). Available from: https://rosap.ntl.bts.gov/view/dot/23703.

[2] Backman H, Nordström R. Improved performance of European long haulage transport. TFK – Institutet för transportforskning; 2002. (TFK report). Available from: https://books.google.se/books?id=5YQMkAEACAAJ.

[3] Woodrooffe J, Ash L. Economic efficiency of long combination transport vehicles in Alberta. Woodrooffe & Associates; 2001. Available from: https://open.alberta.ca/publications/final-report-economic-efficiency-of-long-combination-transport-vehicles-in-alberta.

[4] Dunn AL. Jackknife stability of articulated tractor semitrailer vehicles with high-output brakes and jackknife detection on low coefficient surfaces [dissertation]. Columbus (OH): The Ohio State University; 2003. Available from: http://rave.ohiolink.edu/etdc/view?acc_num=osu1061328963.

[5] Bouteldja M, Koita A, Dolcemascolo V, et al. Prediction and detection of jackknifing problems for tractor semi-trailer. In: Proceedings of the 2006 IEEE Vehicle Power and Propulsion Conference; 2006 Sep 6–8; Windsor, UK: IEEE; 2006. Available from: https://ieeexplore.ieee.org/document/4211300.

[6] Bouteldja M, Cerezo V. Jackknifing warning for articulated vehicles based on a detection and prediction system. In: Proceedings of the 3rd International Conference on Road Safety and Simulation; 2011 Sep 14–16; Indianapolis (IN); Available from: https://onlinepubs.trb.org/onlinepubs/conferences/2011/RSS/3/Bouteldja,M.pdf.

[7] Kaneko T, Kageyama I, Tsunashima H. Braking stability of articulated vehicles on highway. Veh Syst Dyn. 2002;37(sup1):1–11. doi: 10.1080/00423114.2002.11666216

[8] VLK F. Lateral dynamics of commercial vehicle combinations a literature survey. Veh Syst Dyn. 1982;11(5-6):305–324. doi: 10.1080/00423118208968702

[9] Federal Motor Carrier Safety Administration Analysis Division. Large truck and bus crash facts 2020. U.S. Department of Transportation; 2022. Available from: https://www.fmcsa.dot.gov/sites/fmcsa.dot.gov/files/2022-10/LTBCF%202020-v5_FINAL-09-20-2022%20508%2010-3.pdf.

[10] Hac A, Fulk D, Chen H. Stability and control considerations of vehicle-trailer combination. SAE Int J Passeng Cars. 2008;1(1):925–37. doi: 10.4271/2008-01-1228

[11] Erdinc U, Jonasson M, Kati MS, et al. Safe operating envelope based on a single-track model for yaw instability avoidance of articulated heavy vehicles. Veh Syst Dyn. 2023. doi: 10.1080/00423114.2023.2276767

[12] Milliken WF, Milliken DL. Race car vehicle dynamics. Warrendale (PA): SAE International; 1994.

[13] Tremlett AJ, Assadian F, Purdy DJ, et al. Quasi-steady-state linearisation of the racing vehicle acceleration envelope: a limited slip differential example. Veh Syst Dyn. 2014;52(11):1416–1442. doi: 10.1080/00423114.2014.943927

[14] Novi T, Liniger A, Capitani R, et al. Real-time control for at-limit handling driving on a predefined path. Veh Syst Dyn. 2020;58(7):1007–1036. doi: 10.1080/00423114.2019.1605081

[15] van Oort ER, Chu QP, Mulder JA. Maneuver envelope determination through reachability analysis. In: Holzapfel F, Theil S, editors. Advances in Aerospace Guidance, Navigation and Control: Selected Papers of the 1st CEAS Specialist Conference on Guidance, Navigation and Control; 2011 Apr 13–15; Munich, Germany: Springer; 2011. p. 91–102. doi: 10.1007/978-3-642-19817-5.pdf

[16] Lombaerts T, Schuet S, Acosta D, et al. On-line safe flight envelope determination for impaired aircraft. In: Bordeneuve-Guibé J, Drouin A, Roos C, editors. Advances in Aerospace Guidance, Navigation and Control: Selected Papers of the Third CEAS Specialist Conference on Guidance, Navigation and Control; 2015 Apr 13–15; Toulouse, France: Springer; 2015. p. 263–282. doi: 10.1007/978-3-319-17518-8.pdf

[17] Lombaerts T, Schuet S, Wheeler K, et al. Safe maneuvering envelope estimation based on a physical approach. In: Proceedings of the AIAA Guidance, Navigation, and Control (GNC) Conference; 2013 Aug 19-22; Boston (MA): AIAA; 2013. doi: 10.2514/6.2013-4618
[18] Zhang Y, De Visser C, Chu QP. Online safe flight envelope prediction for damaged aircraft: a database-driven approach. In: Proceedings of the AIAA Modeling and Simulation Technologies Conference; 2016 Aug 19–22; Boston, MAL AIAA; 2016. Available from: https://pure.tudelft.nl/ws/portalfiles/portal/10445072/Ye_postprint_2.pdf.
[19] Park JY, Kim N. Design of a safety operational envelope protection system for a submarine. Ocean Eng. 2018;148:602–611. doi: 10.1016/j.oceaneng.2017.11.016Available from: https://www.sciencedirect.com/science/article/pii/S0029801817306832
[20] Prime R, McIntyre M, Reeves D. Implementation of an improved safe operating envelope. In: Proceedings of the International Youth Nuclear Congress; 2008 Sep 20–26; Interlaken, Switzerland: IYNC; 2008. p. 408.1–408.7. Available from: https://inis.iaea.org/collection/NCLCollectionStore/_Public/40/048/40048172.pdf.
[21] Brown M, Funke J, Erlien S, et al. Safe driving envelopes for path tracking in autonomous vehicles. Control Eng Pract. 2017;61:307–316. doi: 10.1016/j.conengprac.2016.04.013Available from: https://www.sciencedirect.com/science/article/pii/S0967066116300831
[22] Cui Q, Ding R, Wei C, et al. Path-tracking and lateral stabilisation for autonomous vehicles by using the steering angle envelope. Veh Syst Dyn. 2021;59(11):1672–1696. doi: 10.1080/00423114.2020.1776344
[23] Bobier CG, Gerdes JC. Staying within the nullcline boundary for vehicle envelope control using a sliding surface. Veh Syst Dyn. 2013;51(2):199–217. doi: 10.1080/00423114.2012.720377
[24] Bobier CG, Gerdes JC. Envelope control: stabilizing within the limits of handling using a sliding surface. In: IFAC Proceedings Volumes. 6th IFAC Symposium on Advances in Automotive Control; 2010 Jul 12–14; Vol. 43(7). Munich, Germany: IFAC; 2010. p. 162–167. Available from: https://www.sciencedirect.com/science/article/pii/S1474667015368233.
[25] Beal C, Bobier C, Gerdes J. Controlling vehicle instability through stable handling envelopes. In: Proceedings of the ASME 2011 Dynamic Systems and Control Conference and Bath/ASME Symposium on Fluid Power and Motion Control; 2011 Oct 31–Nov 2; Arlington (VA): ASME; 2011.
[26] Hansson A, Andersson E, Laine L, et al. Control envelope for limiting actuation of electric trailer in tractor-semitrailer combination. In: Proceedings of the 2022 IEEE 25th International Conference on Intelligent Transportation Systems (ITSC); 2022 Oct 8–12; Macau, China: IEEE; 2022. p. 3886–3893.
[27] Tagesson K, Sundstrom P, Laine L, et al. Real-time performance of control allocation for actuator coordination in heavy vehicles. In: Proceedings of the 2009 IEEE Intelligent Vehicles Symposium; 2009 Jun 3–5; Xi'an, China: IEEE; 2009. p. 685–690.
[28] Pacejka HB. Tyre and vehicle dynamics. 2nd ed. Oxford: Butterworth-Heinemann; 2005.
[29] Fröjd N. Handling analysis and control development of commercial trucks with Volvo Transport Models. Material presented at: MATLAB EXPO 2021; 2021 May 4–5. Available from: https://se.mathworks.com/videos/handling-analysis-and-control-development-of-commercial-trucks-with-volvo-transport-models-1622035211192.html.
[30] Sundström P, Laine L. Validation of VTM model of tractor 4x2 with semitrailer using winter test results from Arjeplog 2011w11 P2685. Gothenburg (SE): Volvo Group Trucks Technology; 2012. (Engineering report; ER-624557).
[31] Kati MS, Fredriksson J, Jacobson B, et al. A feedback-feed-forward steering control strategy for improving lateral dynamics stability of an A-double vehicle at high speeds. Veh Syst Dyn. 2022;60(11):3955–3976. doi: 10.1080/00423114.2021.1988117
[32] RT3000 v3 [Internet]. Oxfordshire (United Kingdom): OXTS; [cited 2023 Jan 5];. Available from: https://www.oxts.com/products/rt3000-v3/.
[33] SIRIUS® [Internet]. Trbovlje (Slovenia): Dewesoft; [cited 2023 Jan 5];. Available from: https://dewesoft.com/products/daq-systems/sirius.

[34] MicroAutoBox II – dSPACE [Internet]. Wixom (MI): dSPACE GmbH; [cited 2023 Jan 5];. Available from: https://www.dspace.com/en/inc/home/products/hw/micautob/microautobox2.cfm.
[35] Circular Tracks – Colmis Proving Ground [Internet]. Arjeplog (Sweden): Colmis AB; [cited 2023 Jan 5];. Available from: https://www.colmis.com/tracks/lake-tracks/.
[36] Schmitt K, Madsen J, Anitescu M, et al. A gaussian process-based approach for handling uncertainty in vehicle dynamics simulation. In: Proceedings of IMECE20082008 ASME International Mechanical Engineering Congress and Exposition; 2008 Nov 2–6; Boston, MA. Vol. 11. 2008. p. 617–628. doi: 10.1115/IMECE2008-66664